Machine Learning Optimization of Majorana Hybrid Nanowires

Matthias Thamm* and Bernd Rosenow
Institut für Theoretische Physik, Universität Leipzig, Brüderstrasse 16, 04103 Leipzig, Germany

(Received 9 August 2022; accepted 21 February 2023; published 15 March 2023)

As the complexity of quantum systems such as quantum bit arrays increases, efforts to automate expensive tuning are increasingly worthwhile. We investigate machine learning based tuning of gate arrays using the covariance matrix adaptation evolution strategy algorithm for the case study of Majorana wires with strong disorder. We find that the algorithm is able to efficiently improve the topological signatures, learn intrinsic disorder profiles, and completely eliminate disorder effects. For example, with only 20 gates, it is possible to fully recover Majorana zero modes destroyed by disorder by optimizing gate voltages.

DOI: 10.1103/PhysRevLett.130.116202

Introduction.—In recent years, increasingly complex quantum devices have been proposed and implemented [1–5], requiring more personnel-intensive tuning. Therefore, it is becoming profitable, and in some cases even necessary, to automate the tuning process [6–8], and machine learning approaches have been found to be very flexible and robust for this purpose [5,7–12]. Especially for the implementation of large scale quantum computation [13–16], efficient tuning of parameters and gates is crucial and numerous automations in quantum dot based qubits have been proposed [6–8,10,11,17–23].

A popular platform for scalable qubit architectures is based on Majorana zero modes (MZMs) in topological superconductors [1,4,24–29], whose advantages are the nonlocal storage of quantum information and its manipulation via anyonic braiding [24–27,30]. MZMs have been proposed to exist in semiconductor-superconductor heterostructures [24,31–34] and many of their predicted signatures have been observed, such as zero-bias conductance peaks [35–38], the fractional Josephson effect [39], and the suppression of even-odd splitting in Coulomb blockade resonances [40]. For a clean wire, it has been theoretically demonstrated that a harmonic potential profile [41] and magnetic field textures [41–44] can make MZMs more robust, and the geometry of Majorana Josephson junctions has been optimized [45]. Nevertheless, disorder remains a crucial problem [46–49], as it can mimic MZM signatures even in the topologically trivial region [46,48,50–53], or destroy the topological phase altogether [54]: a recent study [55] using the "topological gap protocol" [56] involving multiterminal measurements found that due to disorder only about 20% of Majorana devices are expected to have a topological phase.

In this Letter, we present a case study of automatic tuning of a gate array in proximity to a strongly disordered Majorana wire using the covariance matrix adaptation evolution strategy (CMA-ES) [57,58] algorithm. CMA-ES is a machine learning algorithm that does not need system specific information to operate, and is widely applicable for high dimensional optimization problems [59–63]. Crucially, a good metric allows us to improve desirable system properties during optimization. For example, signatures of MZMs can be mimicked by topologically trivial Andreev bound states (ABSs) [53,64–81], which one would like to avoid. We therefore use the amplitude of coherent transmission [82–85] through a Coulomb-blocked Majorana wire as a metric, which has been measured by placing the wire in an arm of an electron interferometer [84], and which allows us to distinguish MZMs from ABSs [83,85]. We find that already 100 to some 1000 amplitude measurements are sufficient to tune the gate array, such that (i) both the localization of the MZMs and the transmission amplitude are significantly improved and (ii) strong potential disorder is compensated.

Setup.—When embedding the Majorana hybrid wire in one arm of an Aharonov-Bohm interferometer (see Fig. 1), the interference part of the current through the interferometer is given by $I_{\mathrm{intf}} = (2e^2/h)|T^{\mathrm{ref}}|A\cos(\phi+\gamma)$, where A and T^{ref} denote the amplitude of coherent transmission through the wire or reference arm, ϕ the magnetic flux, and γ the interference phase at zero magnetic field (for more details see Ref. [86]). Here, we use the CMA-ES algorithm (flow diagram in Fig. 1) to maximize A by tuning the voltages V_j of N_g gates. The algorithm [58] is initialized with a step size $\sigma^{(0)} = 0.1E_{\mathrm{so}}$, correlation matrix $\mathbf{C}^{(0)} = \mathbb{1}$, the corresponding evolution paths $\boldsymbol{s}_{\mathbf{C}}^{(0)} = \mathbf{0}$ and $\boldsymbol{s}_{\sigma}^{(0)} = \mathbf{0}$, and a gate configuration $\boldsymbol{V}_g^{(0)} = \mathbf{0}$. In each iteration, a population of n_{pop} candidate configurations is drawn from a multivariate normal distribution with mean $\boldsymbol{V}_g^{(t)}$ and covariance matrix $(\sigma^{(t)})^2\mathbf{C}^{(t)}$. Then, the metric A is measured for each candidate in the population and the new mean $\boldsymbol{V}_g^{(t+1)}$ is determined as a weighted average of the $\tilde{n}$ best candidates. The new evolution path $\boldsymbol{s}_{\mathbf{C}}^{(t+1)}$ is then the weighted average of the previous path $\boldsymbol{s}_{\mathbf{C}}^{(t)}$ and $\delta\boldsymbol{s}^{(t+1)} = (\boldsymbol{V}_g^{(t+1)} - \boldsymbol{V}_g^{(t)})/\sigma^{(t)}$,

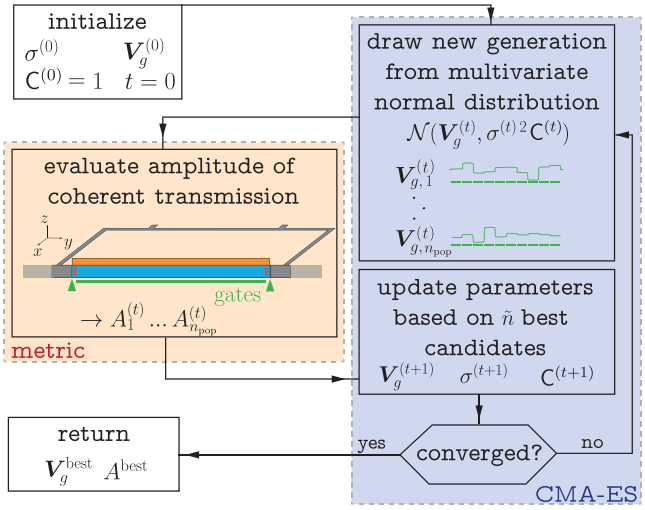

FIG. 1. Schematic diagram of the CMA-ES algorithm [57,58] used to learn an optimal gate voltage configuration that maximizes the amplitude A of coherent transmission through a Majorana hybrid wire embedded into one arm of an Aharonov-Bohm interferometer.

and it determines the new correlation matrix $\mathbf{C}^{(t+1)}$ as a weighted average including $\mathbf{C}^{(t)}$ and $\boldsymbol{s}_{\mathsf{C}}^{(t+1)}[\boldsymbol{s}_{\mathsf{C}}^{(t+1)}]^T$ [58]. The step size $\sigma^{(t)}$ is updated with its own evolution path $\boldsymbol{s}_\sigma^{(t)}$, for details see Refs. [58,86]. We stop optimization if $|A(\boldsymbol{V}_g^{(t+1)}) - A(\boldsymbol{V}_g^{(t)})| < 10^{-8}$ or $\|\boldsymbol{V}_g^{(t+1)} - \boldsymbol{V}_g^{(t)}\| < 10^{-5} E_{\rm so}$.

We Fourier expand the gate voltages

$$V_j = \frac{b_0}{2} + \sum_{k=1}^{\lfloor \frac{N_g-1}{2} \rfloor} a_k \sin\left(\frac{2\pi}{N_g} kj\right) + \sum_{k=1}^{\lfloor \frac{N_g}{2} \rfloor} b_k \cos\left(\frac{2\pi}{N_g} kj\right), \tag{1}$$

as optimizing Fourier components is more robust: since a Fourier component affects all voltages, the algorithm is not distracted by first lowering the gates at the ends which would slightly improve the amplitude, but corresponds to a local optimum only. In the following, we set the average gate voltage $b_0 = 0$ (for $b_0 \neq 0$ see Ref. [86]).

To obtain the spatial profile $V_g(y)$, we assume that the wire is located at a distance $z_{\rm sys}$ from the gates, such that the potential profile is smoothed according to

$$V_g(y) = \mathcal{F}^{-1}\left[\mathrm{e}^{-|q| z_{\rm sys}} \mathcal{F}\left[\sum_{j=1}^{N_g} V_j \chi_j(y)\right]\right], \tag{2}$$

where $\mathcal{F}$ and $\mathcal{F}^{-1}$ are Fourier transform and inverse Fourier transform in the variables y and q, respectively, and $\chi_j(y)$ is 1 if y lies in the region of gate j and 0 otherwise.

We first consider a strictly one-dimensional model for the hybrid wire, and generalize to a more realistic two-dimensional model later. The Majorana wire consisting of a semiconductor with Rashba spin-orbit coupling α_R and a proximity induced s-wave gap Δ is described in the Nambu basis $(d_\uparrow^\dagger(y), d_\downarrow^\dagger(y), d_\downarrow(y), -d_\uparrow(y))$ by the Hamiltonian

$$\begin{aligned}\mathcal{H}_{\rm wire} = \tau_z \Big[&-\frac{\hbar^2 \partial_y^2}{2m^*}\sigma_0 - \mu\sigma_0 - i\hbar\alpha_R \sigma_x \partial_y \\ &+ \delta_{\rm dis}(y)\sigma_0 + V_g(y)\sigma_0 + V_{\rm conf}(y)\sigma_0 \Big] \\ &- E_z \tau_0 \sigma_z + \Delta \tau_x \sigma_0,\end{aligned} \tag{3}$$

with disorder potential $\delta_{\rm dis}$, confinement potential $V_{\rm conf}$, gate potential V_g [see Eq. (2)], and Pauli matrices σ_i and τ_i acting in spin and particle-hole space. Rashba spin-orbit coupling defines a characteristic energy scale $E_{\rm so} = \alpha_R^2 m^*/2 = 0.05$ meV and length scale $l_{\rm so} = \hbar/(\alpha_R m^*) = 0.19$ μm of the system, where $\hbar\alpha = 0.2$ eV Å and $m^* = 0.02 m_e$ are realistic values for InAs [29,35]. We consider wires of length $L = 13\, l_{\rm so}$ on a grid with spacing $a = 0.026\, l_{\rm so}$, with chemical potential $\mu = 1\, E_{\rm so}$, Zeeman energy $E_z = 6\, E_{\rm so}$, and gap $\Delta = 2\, E_{\rm so}$, such that the system is in the topological regime.

We describe disorder by first drawing random numbers δ with standard deviation $\sigma_{\rm dis}$ from a normal distribution, and then introduce a finite correlation length $\lambda_{\rm dis}$ by damping high Fourier modes according to

$$\delta_{\rm dis}(y) = \mathcal{F}^{-1}[\mathrm{e}^{-|q|\lambda_{\rm dis}} \mathcal{F}[\delta(y)]]. \tag{4}$$

Here the case $\lambda_{\rm dis} = 0$ corresponds to onsite disorder.

Wire and leads are connected via steep tunnel barriers of shape $V_{\sigma,V_0}(y) = V_0 \exp[-y^2/(2\sigma^2)]$ with $\sigma = 0.1\, l_{\rm so}$ and $V_0 = 65\, E_{\rm so}$, which are not subject to optimization. For simplicity, we assume the leads as normal conducting and without spin orbit coupling. We treat Coulomb blockade in the Majorana wire using a mean-field approximation, such that adding an extra electron costs a charging energy $E_c = 8\, E_{\rm so}$, and introduce effective energy levels $\varepsilon_{{\rm eff},i}$ containing both charging energy and single particle energies. We consider the system to be tuned to the center between conductance resonances, for a fixed particle number N_0 in the Majorana wire.

Using the Weidenmüller formula [92]

$$\boldsymbol{T} = i\varphi_R^\dagger \Gamma_R U_w \frac{1}{\varepsilon - \mathrm{diag}(\varepsilon_{\rm eff}) - U_w^\dagger \Sigma U_w} U_w^\dagger \Gamma_L \varphi_L, \tag{5}$$

with eigenvectors U_w of the wire Hamiltonian Eq. (3), we determine the transmission amplitude $|T_{\uparrow\uparrow} + T_{\downarrow\downarrow}|$. Here, ε is the energy of incoming electrons in the lead, and self-energies Σ_α, $\Gamma_\alpha = i(\Sigma_\alpha - \Sigma_\alpha^\dagger)$, $\Sigma = \sum_\alpha \Sigma_\alpha$, and

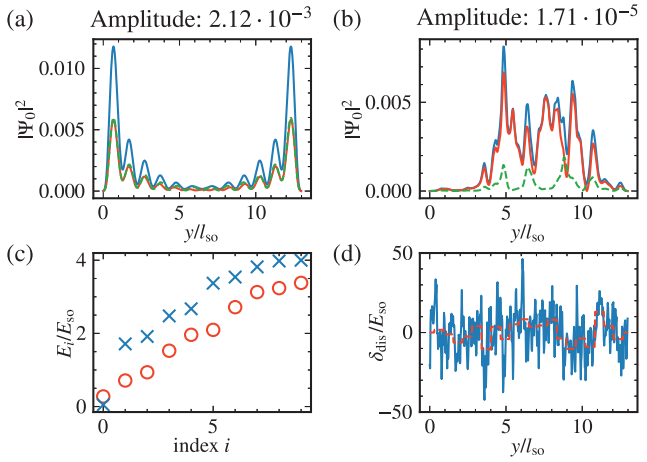

FIG. 2. Reference results for deactivated gates: wave function $|\Psi_0|^2$ of the lowest level (blue), decomposed into hole wave function $|\boldsymbol{v}_0|^2$ (orange) and electron wave function $|\boldsymbol{u}_0|^2$ (green) for the case (a) without disorder, (b) with disorder strength $\sigma_{\mathrm{dis}} = 50\,E_{\mathrm{so}}$ and correlation length $\lambda_{\mathrm{dis}} = 0.052\,l_{\mathrm{so}}$. (c) Energies of the lowest ten Bogoliubov levels for the case without disorder (blue crosses) and with disorder (red circles). (d) Disorder potential along the wire (blue) and average of the disorder over gate regions (dashed, red).

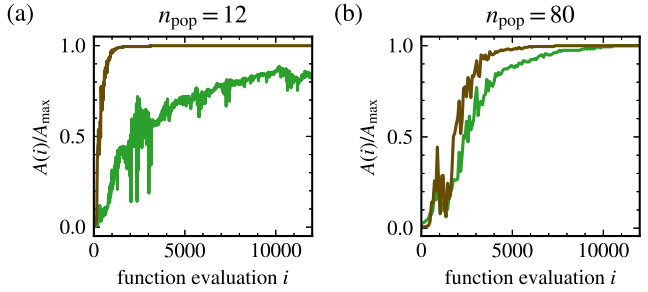

FIG. 3. Convergence speed of the CMA-ES algorithm in the presence of disorder using 20 gates. We consider runs of the CMA-ES algorithm with population sizes (a) $n_{\mathrm{pop}} = 12$ and (b) $n_{\mathrm{pop}} = 80$. In both cases, we consider a "hard" problem (green) with onsite disorder, and an "easier" problem with short range disorder correlations $\lambda_{\mathrm{dis}} = 0.052\,l_{\mathrm{so}}$. The panels depict the degree of convergence $A(i)/A_{\mathrm{max}}$ as a function of the number of function evaluations i (number of amplitude measurements) where A_{max} is the value to which the amplitude ultimately converges.

propagating modes φ_α of lead α are obtained by using the PYTHON package KWANT [93].

A finite temperature can be considered by computing the scattering matrix for different thermally excited states and averaging the transmission amplitude $A = |\langle T_{\uparrow\uparrow} + T_{\downarrow\downarrow}\rangle|$. Denoting the energies of the ABSs by ϵ_1, ϵ_2, the contribution of trivial ABSs to A is suppressed by a factor $1 - \exp[-\beta(\epsilon_1 + \epsilon_2)]$ [83,85,86], as there is destructive interference between the transmission through states with empty and occupied ABSs, respectively. When setting $k_B T = 0.3 E_{\mathrm{so}}$ [94], we find that local optima of A due to ABSs are reliably ignored, and we did not encounter false positives in our optimization runs. For the optimization, we consider transport through the first 10 levels and verify the final results by taking into account 50 levels. We carefully checked that this does not influence the optimization results.

In the absence of disorder and for $V_j \equiv 0$, the lowest level of the wire is approximately at zero energy [see Fig. 2(c)], and the associated wave function $\Psi_0 = (\boldsymbol{u}_0, \boldsymbol{v}_0)$ is localized at the wire ends satisfying the Majorana condition $|\boldsymbol{u}_0(y)| = |\boldsymbol{v}_0(y)|$ (see Fig. 2). When adding strong disorder, both the topological gap and the MZMs are destroyed, and the transmission amplitude is reduced by 2 orders of magnitude.

Optimization results.—To understand the convergence behavior and the influence of the population size n_{pop} on the CMA-ES algorithm, we consider two scenarios: (i) a finite correlation length $\lambda_{\mathrm{dis}} = 0.052\,l_{\mathrm{so}}$ and (ii) onsite disorder, and optimize 20 gates with population sizes $n_{\mathrm{pop}} = 12$ and $n_{\mathrm{pop}} = 80$. In the easier case (i) already the smaller population size is sufficient to achieve fast convergence after less than 1000 function evaluations [brown line Fig. 3(a)], whereas for $n_{\mathrm{pop}} = 80$ about 5 times as many evaluations are necessary [brown line Fig. 3(b)]. In contrast, we find that the more difficult problem (ii) converges poorly in the case of small population sizes, but converges almost as fast as the correlated disorder case for $n_{\mathrm{pop}} = 80$. Thus, if the primary time effort is to perform a function evaluation, we recommend to deviate from the standard value $n_{\mathrm{pop}} = 4 + 3\ln(N_g - 1)$ [95] for the case of a small disorder correlation length.

In the following, we distinguish between (i) optimization in the absence of disorder to improve the localization properties of the MZMs ("wave function engineering"), and (ii) optimization with disorder in the wire. In the case (i) for 20 gates, the transmission amplitude is enhanced by a factor of about 1.6 due to improved MZM localization [Fig. 4(a)] while keeping a sizable topological gap (inset). Here, potentials of the outermost gates are lowered to draw more weight of the wave functions to the wire ends [Fig. 4(c)]. In case (ii) with disorder [cf. Fig. 2(b)], the optimization almost completely restores the MZMs and the topological gap, increasing the transmission amplitude by two orders of magnitude [Fig. 4(b)]. The optimized potential compensates the average disorder [dashed red line Fig. 4(d)], in addition to the zero disorder optimal values [Fig. 4(c)].

We next consider how reliable the optimization is for different disorder correlation lengths, how many gates are necessary, and how strong the dependence on the seed of the CMA-ES random number generator is. For this, we consider 15 different values for the number of gates, from $N_g = 4$ to $N_g = 200$, and three types of disorder, onsite ($\lambda_{\mathrm{dis}} = 0$), $\lambda_{\mathrm{dis}} = 0.052\,l_{\mathrm{so}}$, and $\lambda_{\mathrm{dis}} = 0.52\,l_{\mathrm{so}}$, as well as wave function engineering without disorder. We consider

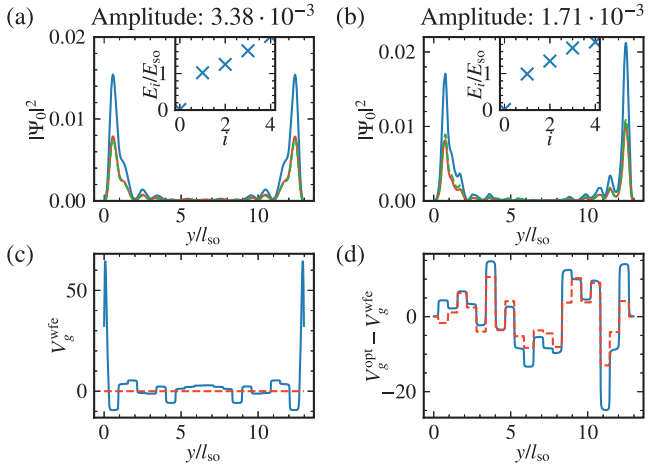

FIG. 4. Optimization of transmission via tuning of 20 gates for a one-dimensional wire in the topological regime with $n_{pop} = 80$. Wave function $|\Psi_0|^2$ of the Majorana level (blue), and the corresponding hole and electron wave functions $|v_0|^2$ (orange), $|\boldsymbol{u}_0|^2$ (green) for (a) no disorder in the wire and (b) disorder strength $\sigma_{dis} = 50\,E_{so}$ and a correlation length $\lambda_{dis} = 0.052\,l_{so}$. The insets depict the energies of the lowest five Bogoliubov levels. Optimized gate potentials in the absence of disorder are shown in (c), and in (d) the difference between optimized potential obtained with and without disorder is shown. The dashed, red line shows the negative average $-V_{dis}^{avg}$ of the disorder potential over the gates, indicating that the algorithm has learned the shape of the disorder potential.

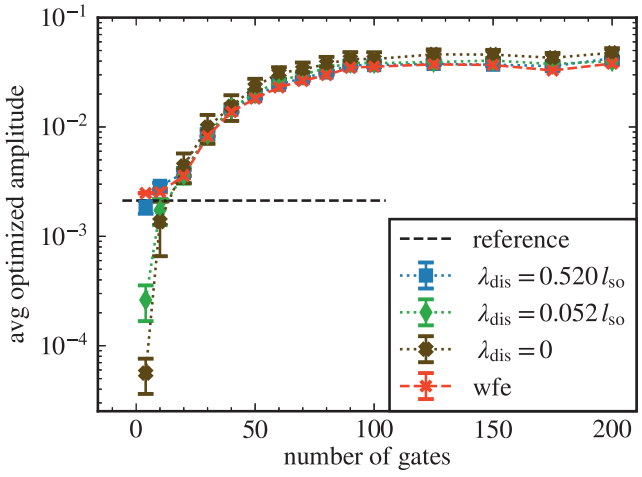

FIG. 5. Optimized transmission amplitude as a function of the number of gates along the wire. Results are shown for disorder strength $\sigma_{dis} = 50\,E_{so}$ and correlation lengths $\lambda_{dis} = 0.52\,l_{so}$ (blue squares), $0.052\,l_{so}$ (green diamonds), 0 (onsite disorder, brown crosses). Red crosses indicate the wave function engineering result obtained for optimization without any disorder in the wire. We show averages over ten realizations of disorder in each case, and an average over 10 seeds of the CMA-ES algorithm in the absence of disorder. The black dashed line shows the reference value obtained without disorder and no optimization.

ten different disorder realizations and average the resulting amplitudes, while in the absence of disorder we average over ten different seeds. We find that for at least 20 gates all disorder profiles can be compensated reliably (see Fig. 5). For too few gates $N_g \leq 10$, disorder with very small correlation length cannot be removed any more. For many gates, $N_g \approx 100$, the amplitude saturates, having increased by 1 order of magnitude as compared to $N_g = 20$, but with the drawback that up to 10^5 function evaluations are needed. We observe a sweet spot $20 \leq N_g \leq 50$, where the number of necessary function evaluations is acceptable and still significant improvements of the amplitude and complete compensation of disorder are possible.

With standard electron beam lithography and Al gates isolated by native oxide it is currently possible to construct such gate arrays of 20 to 50 gates in proximity to Majorana wires of length $L = 13\,l_{so} \approx 2.6$ μm [96,97] considered here. As the CMA-ES algorithm is not gradient based it can escape extended regions in parameter space where the initial amplitude of the disordered wire can be an order of magnitude smaller than the noise level, as long as the transmission amplitude for restored MZMs is an order of magnitude above the noise level [86].

Choice of metric.—Besides the coherent transmission amplitude discussed above, other metrics come to mind that may be easier to determine experimentally, which, however, turn out to cause problems in the optimization process. For example, optimizing the gap $|\varepsilon_1 - \varepsilon_0|$ has the disadvantage that it does not require ε_0 to be small and in addition does not depend on the localization at the wire ends. On the other hand, when minimizing the lowest level ε_0, localization of MZMs is not strengthened, and the gap may vanish or ABSs may be present. Optimizing the incoherent part of the conductance through the wire produces trivial ABSs instead of MZMs by lowering the outermost gates. In principle, multi-terminal measurements are able to distinguish MZMs from ABSs [56]. However, their disadvantage is that there is no obvious single quantity that can be optimized.

Two dimensional case.—We study a wire with length $L_y = 13\,l_{so}$ and width $L_x = 0.39\,l_{so}$, and account for the orbital effect of the magnetic field by adding Peierls phases $e^{-ie/\hbar \int_{r_1}^{r_2} \boldsymbol{A}\cdot d\boldsymbol{r}}$ to the hoppings from site $\boldsymbol{r}_1$ to site $\boldsymbol{r}_2$. We choose a chemical potential $\mu = 63\,E_{so}$ and Zeeman energy $E_z = 6\,E_{so}$ such that the wire in the absence of disorder and gates is in the topological regime with one occupied subband (for a discussion of higher subbands see Ref. [86]). In the presence of strong disorder, the MZMs are destroyed [Fig. 6(a)] and the gap collapses [red circles in Fig. 6(d)], but again optimization with only 20 gates along the wire can restore the MZMs [Fig. 6(b)] as well as the gap [blue crosses in Fig. 6(d)].

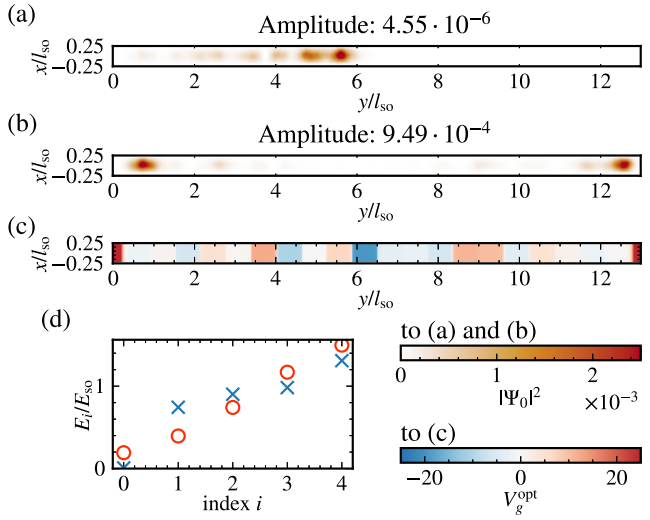

FIG. 6. Optimization of 20 gates along a two-dimensional wire in the topological regime. Wave function $|\Psi_0|^2$ of the lowest level for (a) disorder with $\sigma_{dis} = 150\, E_{so}$ and $\lambda_{dis} = 0.052\, l_{so}$ where all gates are set to zero for reference and (b) optimized gates in the presence of disorder. (c) CMA-ES optimization result for the gate potential that maximizes the transmission amplitude. (d) Energies of the lowest ten Bogoliubov levels for the reference case with disorder (red circles) and for the optimized gate potential (blue crosses). Similarly to the one-dimensional case, the Majorana zero modes, topological gap, and transmission amplitude are restored by the optimized gates.

Conclusions.—We studied machine learning optimization of a gate array using the CMA-ES algorithm. Using the coherent transmission amplitude through a Coulomb blockaded Majorana wire as metric, we find (i) optimization in absence of disorder improves localization of MZMs significantly and (ii) optimization even restores MZMs fully in the case of strong disorder that otherwise destroys the topological phase. We discussed the importance of the choice of an appropriate metric, showed that the number of necessary function evaluations would be experimentally feasible, and demonstrated that a moderate number of gates is sufficient for restoration of MZMs in the presence of disorder. While tuning scalable topological qubits remains a major challenge due to the required number of individually tunable gates, we argue that automated tuning of individual wires and smaller systems can enable proof-of-principle experiments and advance the understanding of disorder effects, with the ultimate goal of scalability in improved materials with lower disorder.

We would like to thank E. van Nieuwenburg, A. Chatterjee, and A. Pöschl for helpful discussions. This work has been funded by the Deutsche Forschungsgemeinschaft (DFG) under Grants No. RO 2247/11-1 and No. 406116891 within the Research Training Group RTG 2522/1.

*Corresponding author.
thamm@itp.uni-leipzig.de

[1] T. Karzig, C. Knapp, R. M. Lutchyn, P. Bonderson, M. B. Hastings, C. Nayak, J. Alicea, K. Flensberg, S. Plugge, Y. Oreg, C. M. Marcus, and M. H. Freedman, Phys. Rev. B **95**, 235305 (2017).
[2] F. Arute *et al.*, Nature (London) **574**, 505 (2019).
[3] D. T. Lennon, H. Moon, L. C. Camenzind, L. Yu, D. M. Zumbühl, G. A. D. Briggs, M. A. Osborne, E. A. Laird, and N. Ares, npj Quantum Inf. **5**, 79 (2019).
[4] Y. Oreg and F. von Oppen, Annu. Rev. Condens. Matter Phys. **11**, 397 (2020).
[5] N. Ares, Nat. Rev. Mater. **6**, 870 (2021).
[6] T. A. Baart, P. T. Eendebak, C. Reichl, W. Wegscheider, and L. M. K. Vandersypen, Appl. Phys. Lett. **108**, 213104 (2016).
[7] D. L. Craig, H. Moon, F. Fedele, D. T. Lennon, B. van Straaten, F. Vigneau, L. C. Camenzind, D. M. Zumbühl, G. A. D. Briggs, M. A. Osborne, D. Sejdinovic, and N. Ares, arXiv:2111.11285.
[8] J. Ziegler, T. McJunkin, E. S. Joseph, S. S. Kalantre, B. Harpt, D. E. Savage, M. G. Lagally, M. A. Eriksson, J. M. Taylor, and J. P. Zwolak, arXiv:2108.00043.
[9] A. Frees, J. K. Gamble, D. R. Ward, R. Blume-Kohout, M. A. Eriksson, M. Friesen, and S. N. Coppersmith, Phys. Rev. Appl. **11**, 024063 (2019).
[10] S. S. Kalantre, J. P. Zwolak, S. Ragole, X. Wu, N. M. Zimmerman, M. D. Stewart, and J. M. Taylor, npj Quantum Inf. **5**, 6 (2019).
[11] H. Moon, D. T. Lennon, J. Kirkpatrick, N. M. van Esbroeck, L. C. Camenzind, L. Yu, F. Vigneau, D. M. Zumbühl, G. A. D. Briggs, M. A. Osborne, D. Sejdinovic, E. A. Laird, and N. Ares, Nat. Commun. **11**, 4161 (2020).
[12] H.-C. Ruiz Euler, M. N. Boon, J. T. Wildeboer, B. van de Ven, T. Chen, H. Broersma, P. A. Bobbert, and W. G. van der Wiel, Nat. Nanotechnol. **15**, 992 (2020).
[13] T. D. Ladd, F. Jelezko, R. Laflamme, Y. Nakamura, C. Monroe, and J. L. O'Brien, Nature (London) **464**, 45 (2010).
[14] R. Hanson, L. P. Kouwenhoven, J. R. Petta, S. Tarucha, and L. M. K. Vandersypen, Rev. Mod. Phys. **79**, 1217 (2007).
[15] C. Kloeffel and D. Loss, Annu. Rev. Condens. Matter Phys. **4**, 51 (2013).
[16] L. M. K. Vandersypen, H. Bluhm, J. S. Clarke, A. S. Dzurak, R. Ishihara, A. Morello, D. J. Reilly, L. R. Schreiber, and M. Veldhorst, npj Quantum Inf. **3**, 34 (2017).
[17] T. Botzem, M. D. Shulman, S. Foletti, S. P. Harvey, O. E. Dial, P. Bethke, P. Cerfontaine, R. P. G. McNeil, D. Mahalu, V. Umansky, A. Ludwig, A. Wieck, D. Schuh, D. Bougeard, A. Yacoby, and H. Bluhm, Phys. Rev. Appl. **10**, 054026 (2018).
[18] J. D. Teske, S. S. Humpohl, R. Otten, P. Bethke, P. Cerfontaine, J. Dedden, A. Ludwig, A. D. Wieck, and H. Bluhm, Appl. Phys. Lett. **114**, 133102 (2019).
[19] A. R. Mills, M. M. Feldman, C. Monical, P. J. Lewis, K. W. Larson, A. M. Mounce, and J. R. Petta, Appl. Phys. Lett. **115**, 113501 (2019).
[20] R. Durrer, B. Kratochwil, J. V. Koski, A. J. Landig, C. Reichl, W. Wegscheider, T. Ihn, and E. Greplova, Phys. Rev. Appl. **13**, 054019 (2020).

[21] N. M. van Esbroeck, D. T. Lennon, H. Moon, V. Nguyen, F. Vigneau, L. C. Camenzind, L. Yu, D. M. Zumbühl, G. A. D. Briggs, D. Sejdinovic, and N. Ares, New J. Phys. **22**, 095003 (2020).

[22] F. Fedele, A. Chatterjee, S. Fallahi, G. C. Gardner, M. J. Manfra, and F. Kuemmeth, PRX Quantum **2**, 040306 (2021).

[23] O. Krause, A. Chatterjee, F. Kuemmeth, and E. van Nieuwenburg, SciPost Phys. **13**, 084 (2022).

[24] J. Alicea, Y. Oreg, G. Refael, F. von Oppen, and M. P. A. Fisher, Nat. Phys. **7**, 412 (2011).

[25] D. J. Clarke, J. D. Sau, and S. Tewari, Phys. Rev. B **84**, 035120 (2011).

[26] T. Hyart, B. van Heck, I. C. Fulga, M. Burrello, A. R. Akhmerov, and C. W. J. Beenakker, Phys. Rev. B **88**, 035121 (2013).

[27] S. D. Sarma, M. Freedman, and C. Nayak, npj Quantum Inf. **1**, 15001 (2015).

[28] D. Aasen, M. Hell, R. V. Mishmash, A. Higginbotham, J. Danon, M. Leijnse, T. S. Jespersen, J. A. Folk, C. M. Marcus, K. Flensberg, and J. Alicea, Phys. Rev. X **6**, 031016 (2016).

[29] R. M. Lutchyn, E. P. A. M. Bakkers, L. P. Kouwenhoven, P. Krogstrup, C. M. Marcus, and Y. Oreg, Nat. Rev. Mater. **3**, 52 (2018).

[30] S. Vijay and L. Fu, Phys. Rev. B **94**, 235446 (2016).

[31] A. Y. Kitaev, Phys. Usp. **44**, 131 (2001).

[32] R. M. Lutchyn, J. D. Sau, and S. Das Sarma, Phys. Rev. Lett. **105**, 077001 (2010).

[33] Y. Oreg, G. Refael, and F. von Oppen, Phys. Rev. Lett. **105**, 177002 (2010).

[34] J. D. Sau, S. Tewari, R. M. Lutchyn, T. D. Stanescu, and S. Das Sarma, Phys. Rev. B **82**, 214509 (2010).

[35] V. Mourik, K. Zuo, S. M. Frolov, S. R. Plissard, E. P. A. M. Bakkers, and L. P. Kouwenhoven, Science **336**, 1003 (2012).

[36] A. Das, Y. Ronen, Y. Most, Y. Oreg, M. Heiblum, and H. Shtrikman, Nat. Phys. **8**, 887 (2012).

[37] M. T. Deng, C. L. Yu, G. Y. Huang, M. Larsson, P. Caroff, and H. Q. Xu, Nano Lett. **12**, 6414 (2012).

[38] F. Nichele, A. C. C. Drachmann, A. M. Whiticar, E. C. T. O'Farrell, H. J. Suominen, A. Fornieri, T. Wang, G. C. Gardner, C. Thomas, A. T. Hatke, P. Krogstrup, M. J. Manfra, K. Flensberg, and C. M. Marcus, Phys. Rev. Lett. **119**, 136803 (2017).

[39] L. P. Rokhinson, X. Liu, and J. K. Furdyna, Nat. Phys. **8**, 795 (2012).

[40] S. M. Albrecht, A. P. Higginbotham, M. Madsen, F. Kuemmeth, T. S. Jespersen, J. Nygård, P. Krogstrup, and C. M. Marcus, Nature (London) **531**, 206 (2016).

[41] S. Boutin, J. Camirand Lemyre, and I. Garate, Phys. Rev. B **98**, 214512 (2018).

[42] J. Klinovaja, P. Stano, and D. Loss, Phys. Rev. Lett. **109**, 236801 (2012).

[43] N. Mohanta, T. Zhou, J.-W. Xu, J. E. Han, A. D. Kent, J. Shabani, I. Žutić, and A. Matos-Abiague, Phys. Rev. Appl. **12**, 034048 (2019).

[44] S. Turcotte, S. Boutin, J. C. Lemyre, I. Garate, and M. Pioro-Ladrière, Phys. Rev. B **102**, 125425 (2020).

[45] A. Melo, T. Tanev, and A. R. Akhmerov, arXiv:2205.05689.

[46] H. Zhang *et al.*, Nat. Commun. **8**, 16025 (2017).

[47] S. Ahn, H. Pan, B. Woods, T. D. Stanescu, and S. D. Sarma, Phys. Rev. Mater. **5**, 124602 (2021).

[48] S. Das Sarma and H. Pan, Phys. Rev. B **103**, 195158 (2021).

[49] P. Yu, J. Chen, M. Gomanko, G. Badawy, Bakkers, E. P. A. M., K. Zuo, V. Mourik, and S. M. Frolov, Nat. Phys. **17**, 482 (2021).

[50] D. Bagrets and A. Altland, Phys. Rev. Lett. **109**, 227005 (2012).

[51] D. I. Pikulin, J. P. Dahlhaus, M. Wimmer, H. Schomerus, and C. W. J. Beenakker, New J. Phys. **14**, 125011 (2012).

[52] J. Liu, A. C. Potter, K. T. Law, and P. A. Lee, Phys. Rev. Lett. **109**, 267002 (2012).

[53] H. Pan and S. Das Sarma, Phys. Rev. Res. **2**, 013377 (2020).

[54] S. Takei, B. M. Fregoso, H.-Y. Hui, A. M. Lobos, and S. Das Sarma, Phys. Rev. Lett. **110**, 186803 (2013).

[55] M. Aghaee, A. Akkala, Z. Alam, R. Ali, A. A. Ramirez, M. Andrzejczuk, A. E. Antipov, M. Astafev, B. Bauer, J. Becker *et al.*, arXiv:2207.02472.

[56] D. I. Pikulin, B. van Heck, T. Karzig, E. A. Martinez, B. Nijholt, T. Laeven, G. W. Winkler, J. D. Watson, S. Heedt, M. Temurhan *et al.*, arXiv:2103.12217.

[57] N. Hansen and A. Ostermeier, Evol. Comput. **9**, 159 (2001).

[58] N. Hansen, S. D. Müller, and P. Koumoutsakos, Evol. Comput. **11**, 1 (2003).

[59] N. Hansen, in *Towards a New Evolutionary Computation*, Studies in Fuzziness and Soft Computing, edited by J. A. Lozano, E. Bengoetxea, I. Inza, and P. Larrañaga (Springer Berlin, Heidelberg, 2006), pp. 75–102.

[60] *Towards a New Evolutionary Computation: Advances in the Estimation of Distribution Algorithms*, edited by J. A. Lozano, E. Bengoetxea, I. Inza, and P. Larrañaga, Studies in Fuzziness and Soft Computing, Vol. 192 (Springer Berlin, Heidelberg, 2006).

[61] I. Loshchilov and F. Hutter, arxiv:1604.07269.

[62] M. Willjuice Iruthayarajan and S. Baskar, Expert Syst. Appl. **37**, 5775 (2010).

[63] I. Loshchilov, M. Schoenauer, and M. Sebag, in *Proceedings of the 15th Annual Conference Companion on Genetic and Evolutionary Computation* (Association for Computing Machinery, New York, 2013), pp. 1177–1184.

[64] G. Kells, D. Meidan, and P. W. Brouwer, Phys. Rev. B **86**, 100503(R) (2012).

[65] E. Prada, P. San-Jose, and R. Aguado, Phys. Rev. B **86**, 180503(R) (2012).

[66] D. Rainis, L. Trifunovic, J. Klinovaja, and D. Loss, Phys. Rev. B **87**, 024515 (2013).

[67] J. Cayao, E. Prada, P. San-Jose, and R. Aguado, Phys. Rev. B **91**, 024514 (2015).

[68] P. San-Jose, J. Cayao, E. Prada, and R. Aguado, Sci. Rep. **6**, 21427 (2016).

[69] J. Chen, P. Yu, J. Stenger, M. Hocevar, D. Car, S. R. Plissard, E. P. A. M. Bakkers, T. D. Stanescu, and S. M. Frolov, Sci. Adv. **3**, e1701476 (2017).

[70] C.-X. Liu, J. D. Sau, T. D. Stanescu, and S. Das Sarma, Phys. Rev. B **96**, 075161 (2017).

[71] F. Peñaranda, R. Aguado, P. San-Jose, and E. Prada, Phys. Rev. B **98**, 235406 (2018).

[72] J. Avila, F. Peñaranda, E. Prada, P. San-Jose, and R. Aguado, Commun. Phys. **2**, 133 (2019).
[73] C.-K. Chiu and S. Das Sarma, Phys. Rev. B **99**, 035312 (2019).
[74] J. Chen, B. D. Woods, P. Yu, M. Hocevar, D. Car, S. R. Plissard, E. P. A. M. Bakkers, T. D. Stanescu, and S. M. Frolov, Phys. Rev. Lett. **123**, 107703 (2019).
[75] B. D. Woods, J. Chen, S. M. Frolov, and T. D. Stanescu, Phys. Rev. B **100**, 125407 (2019).
[76] A. Vuik, B. Nijholt, A. Akhmerov, and M. Wimmer, SciPost Phys. **7**, 061 (2019).
[77] O. A. Awoga, J. Cayao, and A. M. Black-Schaffer, Phys. Rev. Lett. **123**, 117001 (2019).
[78] O. Dmytruk, D. Loss, and J. Klinovaja, Phys. Rev. B **102**, 245431 (2020).
[79] E. Prada, P. San-Jose, M. W. de Moor, A. Geresdi, E. J. Lee, J. Klinovaja, D. Loss, J. Nygård, R. Aguado, and L. P. Kouwenhoven, Nat. Rev. Phys. **2**, 575 (2020).
[80] M. Valentini, F. Peñaranda, A. Hofmann, M. Brauns, R. Hauschild, P. Krogstrup, P. San-Jose, E. Prada, R. Aguado, and G. Katsaros, Science **373**, 82 (2021).
[81] H. Zhang *et al.*, arXiv:2101.11456.
[82] L. Fu, Phys. Rev. Lett. **104**, 056402 (2010).
[83] M. Hell, K. Flensberg, and M. Leijnse, Phys. Rev. B **97**, 161401(R) (2018).
[84] A. M. Whiticar, A. Fornieri, E. C. T. O'Farrell, A. C. C. Drachmann, T. Wang, C. Thomas, S. Gronin, R. Kallaher, G. C. Gardner, M. J. Manfra, C. M. Marcus, and F. Nichele, Nat. Commun. **11**, 3212 (2020).
[85] M. Thamm and B. Rosenow, Phys. Rev. Res. **3**, 023221 (2021).
[86] See Supplemental Material at http://link.aps.org/supplemental/10.1103/PhysRevLett.130.116202, which includes Refs. [87–91] for additional details and numerical results.
[87] G. W. Winkler, A. E. Antipov, B. van Heck, A. A. Soluyanov, L. I. Glazman, M. Wimmer, and R. M. Lutchyn, Phys. Rev. B **99**, 245408 (2019).
[88] P. Wójcik and M. P. Nowak, Phys. Rev. B **97**, 235445 (2018).
[89] F. Pientka, G. Kells, A. Romito, P. W. Brouwer, and F. von Oppen, Phys. Rev. Lett. **109**, 227006 (2012).
[90] Nikolaus Hansen, yoshihikoueno, ARF1, Kento Nozawa, Matthew Chan, Youhei Akimoto, and Dimo Brockhoff, CMA-ES/pycma: r3.1.0, Zenodo, 10.5281/zenodo.5002422 (2021).
[91] N. Hansen, arXiv:1604.00772.
[92] C. Mahaux and H. A. Weidenmüller, Phys. Rev. **170**, 847 (1968).
[93] C. W. Groth, M. Wimmer, A. R. Akhmerov, and X. Waintal, New J. Phys. **16**, 063065 (2014).
[94] We note that tuning the Majorana wire at a somewhat higher temperature does not preclude using it at ultralow temperatures for optimized performance in quantum information applications.
[95] N. Hansen, Y. Akimoto, and P. Baudis, CMA-ES/pycma on Github, Zenodo, 10.5281/zenodo.2559634 (2019).
[96] A. Mills, D. Zajac, M. Gullans, F. Schupp, T. Hazard, and J. Petta, Nat. Commun. **10**, 1063 (2019).
[97] A. Pöschl, Nonlocal transport signatures of Andreev Bound States, Ph.D. thesis, Center for Quantum Devices, Niels Bohr Institute, University of Copenhagen, 2022.